Surfactant-Resisted Assembly of Fe-Containing Nanoparticles for Site-Specific Growth of SWNTs on Si Surface

Maoshuai He, Xing Ling, Jin Zhang,* and Zhongfan Liu*

Key Laboratory for the Physics and Chemistry of Nanodevices, Centre for Nanoscale Science and Technology (CNST), College of Chemistry and Molecular Engineering, Peking University, Beijing 100871, P.R. China

Received: March 4, 2005; In Final Form: April 2, 2005

This paper describes a facile approach to the site-specific growth of single-walled carbon nanotubes (SWNTs) on silicon surfaces by chemical vapor deposition (CVD). The approach is based on the use of a surfactant as a resist to define patterns of silicon oxide nanodomains onto which nanoparticles of iron hydroxide ($Fe(OH)_3$), 1−5 nm diameter, could be deposited. In base growth mode, the SWNTs can grow from the oxide nanodomains. By controlling the location of oxide nanodomains, site-specific growth could be obtained. The iron hydroxide nanoparticles were prepared by hydrolysis of ferric chloride ($FeCl_3$). Patterned hydroxylated silicon oxide nanodomains were created by scanning probe oxidation (SPO) of silicon substrates modified with aminopropyltrimethoxysilane (APTMS, $H_2N(CH_2)_3Si(OCH_3)_3$). Due to electrostatic interaction, $Fe(OH)_3$ nanoparticles can be selectively deposited on hydroxyl groups present on silicon oxide nanodomains. To inhibit the assembly of the nanoparticles on a APTMS-coated silicon surface, sodium dodecyl sulfate (SDS) was introduced, which restricted deposition to the hydroxylated nanodomains. A model mechanism for the selective deposition mechanism has been proposed. It was possible to convert the patterned $Fe(OH)_3$ nanoparticles to iron oxide, which served as a catalyst for the site-specific growth of SWNTs. Raman spectroscopy and AFM were used to characterize the nanotubes on the Si substrate. This will offer the possibility for future integration with conventional microelectronics as well as the development of novel devices.

Introduction

The unique electrical and physical properties of single-walled carbon nanotubes (SWNTs) make them valuable for numerous applications.[1] Significant progress has been made in both their production and application in a wide variety of fields.[2−7] Arc-discharge, laser ablation, and chemical vapor deposition (CVD) methods have all been actively investigated for bulk growth of high-purity SWNTs.[2−4] Although there is little selectively in controlling the properties of the products, many SWNT-based devices have been demonstrated, such as quantum wires,[5] field effect transistors,[6] and room-temperature single-electron transistors.[7]

Normally, manufacture of SWNT-based nanodevices requires undamaged individual SWNTs with a high purity dispersed on a solid substrate.[5−7] However, SWNTs are typically synthesized with polydisperse lengths in the micrometer range, usually considerably tangled.[8] In addition, the as-produced SWNTs often contained impurities such as catalysts and amorphous carbon, which must be removed for many applications. However, post-manufacture purification with highly oxidative chemicals and ultrasonication also tends to introduce defects to SWNTs.[9] These problems can be overcome to some extent by growing isolated SWNTs by CVD on solid surface, using preformed monodisperse catalyst nanoparticles.[10−12]

The key parameters that influence the qualities of SWNTs grown on surfaces are the monodispersity of transition metal nanoparticles known to catalyze nanotube growth (Fe, Co, and Ni), an appropriate carbon source (C_2H_4, CO, CH_4, etc.), and strict temperature control. Considerable efforts have been made to grow SWNTs on surfaces with use of isolated catalyst nanoparticles or clusters of identical particles.[13−15] By using "fast heating" or applying an appropriate electrical field during the growth process, the direction of SWNT growth can also be controlled.[13−15] These approaches are paramount for the development of a reliable and scalable process for making a large number of devices.

To fabricate SWNT-based devices, it is necessary to determine the location of SWNTs. Isolated SWNTs have been fabricated by CVD on catalysts in patterns obtained by standard lithographic techniques, for example, electron-beam[16] and photolithographic techniques.[17] However, catalyst supports typically used for SWNT growth have consisted of powdery materials supporting attached metal nanoparticles. Since these are difficult to characterize by microscopy, the size of catalytic nanoparticles is difficult to control.[8] This makes it difficult to determine size and location of SWNTs since they do not originate from the preformed catalyst nanoparticles. Since the CVD reaction process is comprised of decomposition of carbon source molecules, re-formation of carbon atoms into nanoparticles, and their precipitation into a crystalline tubular form, precise positioning of well-characterized catalyst nanoparticles can thus produce site-specific growth of SWNTs.

With combined use of self-assembled monolayers (SAMs) and nanofabrication technique (for example, electron beam lithography[18] or photolithography[19] or SPO[20]), coplanar nanostructures consisting of two different types of functional groups could be easily fabricated and used as molecular linkers for the area-selective immobilization of catalytic materials. Among them, SPO is highly promising because of its widespread availability, and it thus has been intensively studied.[20] Most of this work focused on producing nanoparticles with relatively large diameters (normally >10 nm); it is more difficult to

10.1021/jp051127j CCC: $30.25
Published on Web 04/30/2005

assemble sub-10 nm nanoparticles at lithographically defined precise locations.[21]

In the work reported here, using SDS as a resist we have demonstrated the combination of SPO and self-assembly techniques for selectively positioning colloidal $Fe(OH)_3$ nanoparticles of small diameter (1−5 nm). A mechanism for the resist effect of surfactant during the nanoparticle assembly process has been proposed. Decomposition of the assembled $Fe(OH)_3$ nanoparticles was effected to produce iron oxide nanoparticles for catalytic growth of SWNTs in a CVD system. With use of a base-growth mode, site-specific growth of SWNTs on Si substrate was achieved.

Experimental Section

Preparation of $Fe(OH)_3$ Colloid. $Fe(OH)_3$ colloid was prepared by hydrolysis of anhydrous $FeCl_3$. $FeCl_3$ aqueous solution (5.0 mL, 0.10 mol·dm^{-3}) was added dropwise to 175 mL of deionized water heated to just over 80 °C, then the solution was allowed to stand at the same temperature for another 2 h. Magnetic stirring was performed throughout the process. The pH value of the as-prepared $Fe(OH)_3$ colloid was ∼2.0.

Preparation of APTMS and Octadecyltrimethoxysilane (OTS, $(CH_3O)_3Si(CH_2)_{17}CH_3$) SAMs. The Si (111) wafers were cleaned in acetone, ethanol, deionized water, and piranha solution (H_2SO_4:H_2O_2 = 7:3, v/v). After being washed in deionized water and dried by ultrapure N_2, they were immersed in a fresh solution of 0.1 vol % of APTMS in ethanol for 25 min. The samples were then rinsed in deionized water and heated at 110 °C for 40 min. An OTS SAM was assembled on the Si substrate, using CVD.[22] Briefly, cleaned substrate wafers and a weighing bottle (2 cm2 cm) filled with 100 μL of OTS were placed together in a 78 cm^3 (3 cm × 11 cm) cylindrical Teflon container. The container was then sealed and placed in an oven at 150 °C for 2 h.

Fabrication of Nanopatterns by SPO. SPO was carried out with a Multimode nanoscope III in contact mode, using TiN coated silicon tips. With feedback switched on, the probe was programmed to move to a patterned series of predefined positions. To pass current through the SAM at these sites, a DC bias voltage was applied between the conductive AFM probe and Si substrate that served as cathode and anode, respectively.[23]

Modification of $Fe(OH)_3$ Colloid by SDS. A 50.0 mL sample of as-prepared $Fe(OH)_3$ colloidal solution was added dropwise to 5.0 mL of sodium dodecyl sulfate (SDS) solution (0.02 M) with magnetic stirring.

Assembly of Nanoparticles. Si wafers were immersed in $Fe(OH)_3$- or SDS-containing $Fe(OH)_3$ solution for 5 min, followed by washing copiously with water. They were blown dry with ultra pure N_2 prior to characterization.

Growth of SWNTs. The substrate was first annealed in air at 600 °C for half an hour to activate the catalyst. CVD growth was then carried out at 900 °C under a flow of CH_4 at 600 standard cubic centimeters per minute (sccm). Before growth, argon (Ar) was introduced to the reaction system at 300 sccm, and when the furnace had reached the require temperature, Ar was replaced by CH_4 for 10 min. After growth, the system was cooled to room temperature under Ar.

Characterization of SWNTs. To characterize SWNTs grown on the Si substrate, scanning electron microscopy (SEM, XL30S-FEG, 10 kV), AFM (Digital Instrument, nanoscope III), and Raman spectroscopy (Renishaw micro-Raman 1000, 632.8 nm) were employed.

Results and Discussions

As described in Figure 1, the approach described here for site-specific growth of SWNTs on silicon surfaces comprised three principal steps: (1) preparation of nanoscale domains, (2) deposition of catalytic nanoparticles, and (3) SWNT growth with CVD. An APTMS monolayer was deposited on the Si substrate (Figure 1a), applying a bias voltage to the AFM probe/sample junction. In this way, a nanopattern was produced by the probe tip on the APTMS-coated Si substrate (Figure 1b). With use of sodium dodecyl sulfate (SDS), as a resist coating, iron hydroxide ($Fe(OH)_3$) colloidal nanoparticles were selectively anchored on oxide domains (Figure 1c). After being washed and annealed in air, $Fe(OH)_3$ was be converted to iron oxide that subsequently catalyzed SWNT growth at the predetermined pattern locations (Figure 1d).

A. Preparation of Nanoscale Domains. Figure 2a is an AFM image of a patterned APTMS-coated Si sample after oxidation by an SPM probe. Applying a bias voltage across the probe/sample junction, the APTMS molecules were locally removed from the probe-scanned area. At the same time, the underlying substrate was converted to silicon oxide (SiO_x) that most likely terminated with hydroxyl (−OH) groups. Owing to volume expansion of the oxide layer, the probe-scanned regions slightly protruded from the surrounding unscanned area. As indicated in Figure 2b, the height of the oxide domains over surrounding areas is about 2.2 nm. Degradation of organosilane layers is most likely due to water electrolysis and related electrochemical reactions induced beneath the tip. The size and height of oxide domains depended on many parameters, such as tip geometry, ambient humidity, and duration of applied voltage. The dependence of oxide dot size on organosilane SAM was similar to that of previous reports:[24] it increased with higher humidity, larger voltage, and longer pulse duration. In our SPO process, humidity was usually in the range of 20% to 40%, pulse duration was 500 ms for all runs, and we controlled the size of the oxide dot by adjusting bias voltage (8−16 V).

B. Catalytic Nanoparticle Adsorption. Coplanar nanostructures exhibiting two different terminal groups were thus fabricated. Areas that were not modified by the probe would be covered with amino-terminated APTMS. Since their pK_a is ∼7.5,[25] which is much higher than the pH value of $Fe(OH)_3$ solution (∼2.0), most of the amino groups would be protonated in $Fe(OH)_3$ solution. It was therefore postulated that few nanoparticles would deposit on APTMS since both surface and nanoparticles would exhibit a positive charge. Figure 2c is an AFM image of APTMS−SAM sample after being immersed in $Fe(OH)_3$ solution for 5 min followed by extensive washing in deionized water. Clearly many nanoparticles were attached to the APTMS−Si substrate. There are several possible reasons for this: First, sub-5 nm $Fe(OH)_3$ nanoparticles are fairly mobile due to their high surface free energy,[26] and their adsorption onto the substrate could lower the interfacial surface energy. Second, positively charged $Fe(OH)_3$ colloidal nuclei (due to the adsorption of FeO^+ stabilizer) may be adsorbed onto the APTMS surface via hydrogen bonding ($FeO\cdots H\cdots NH_2$). Third, the existence of very small pinholes in the surface layer cannot be excluded.[24]

In an effort to solve this problem, a surfactant, SDS, was introduced into the system to inhibit adsorption of nanoparticles on APTMS−Si substrate. Using AFM adhesion force measurement, the adsorption behavior of SDS on charge-regulated substrates has been characterized by Hu et al.[27] SDS adsorption was investigated by measuring the double-layer forces between a negative silica AFM probe and either a positively charged or

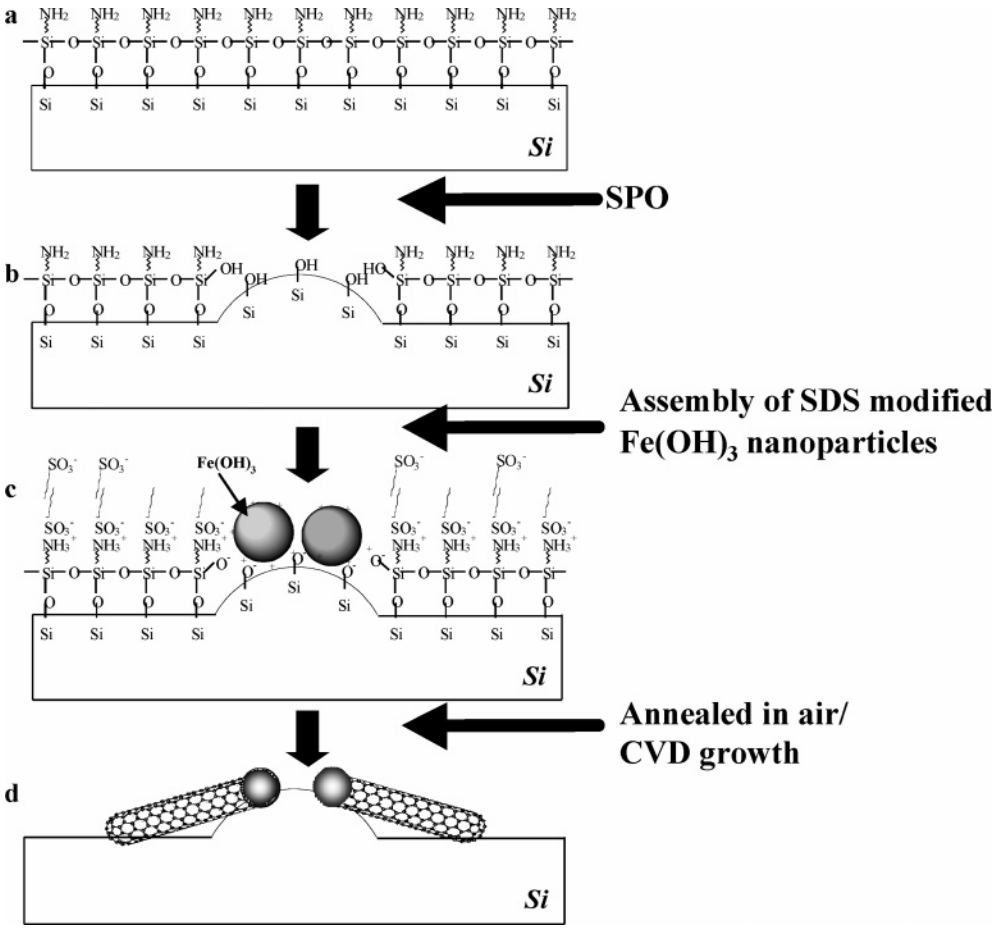

Figure 1. Schematic sketch of the process for positioning $Fe(OH)_3$ nanoparticles onto prepared SAM template and growing SWNTs from these catalyst nanoparticles. (a) A layer of APTMS monolayer was assembled onto Si wafer. (b) Nanodegradation of SAM and the underlying Si substrate by SPO. (c). Assembly of nanoparticles onto a defined area with resist of SDS. (d) CVD growth of SWNTs from the iron-containing catalyst.

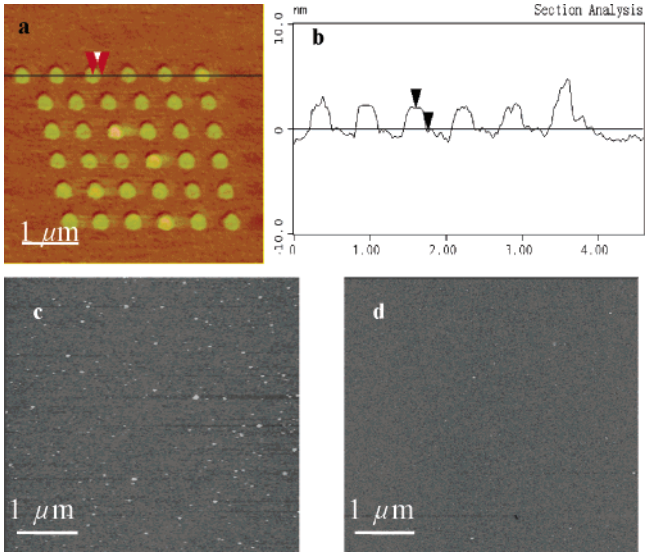

Figure 2. (a) An AFM image of as-fabricated nanodomain arrays (6 × 6) and (b) its section analysis, with heights about 2.2 nm. (c) A typical AFM image of APTMS-coated Si substrate after immersed in $Fe(OH)_3$ solution for 5 min. (d) A typical AFM image of APTMS-coated Si substrate after immersion in SDS-modified $Fe(OH)_3$ solution for 5 min.

hydrophobic SAM-covered gold substrate over a broad range of SDS concentrations. Although it was concluded that the formation of a compact uniform SDS "hemi-micelle" or bilayerlike layer did not occur, SDS was adsorbed and served as a resist to subsequently inhibit the adsorption of $Fe(OH)_3$ nanoparticles on the bulk APTMS−Si substrate. As demonstrated in Figure 2d, an APTMS−Si sample was immersed for 5 min in SDS containing $Fe(OH)_3$ solution. After being washed in deionized water and dried with high-purity N_2, only a few nanoparticles still remained anchored on the surface. In contrast nanoparticles have great affinity to the probe-scanned regions terminated with −OH. Figure 3 shows AFM images of nanoparticles selectively deposited onto the probe-scanned nanodomains after immersion in SDS-containing $Fe(OH)_3$ solution for 5 min. A submonolayer of nanoparticles is seen to spatially arrange on probe scanned lines while almost no nanoparticles are seen on the surrounding amino-covered substrate (Figure 3a). From Figure 3d, it is apparent that only one to three nanoparticles were adsorbed onto each probe-defined domain, suggesting that the size of the oxide dots is almost a critical size for the assembly of $Fe(OH)_3$ nanoparticles. If the diameter is smaller than this critical value, the adsorption probability of $Fe(OH)_3$ nanoparticle would be less than 100%. The result is consistent with many research reports,[24] the smaller the oxide domains, the more difficult it is for the nanoparticles to adsorb. With a decrease in the size of oxide patterns, fewer nanoparticles assembled onto the probe-scanned areas (Figure 3b,c,d).

The effect of SDS molecules during nanoparticle deposition can be described as follows: First the anionic surfactant, SDS, would have a strong interaction with positively charged $Fe(OH)_3$ nanoparticles. This interaction would greatly decrease the surface free energy of $Fe(OH)_3$ nanoparticles and reduce the mobility of nanoparticles on the substrate. More importantly,

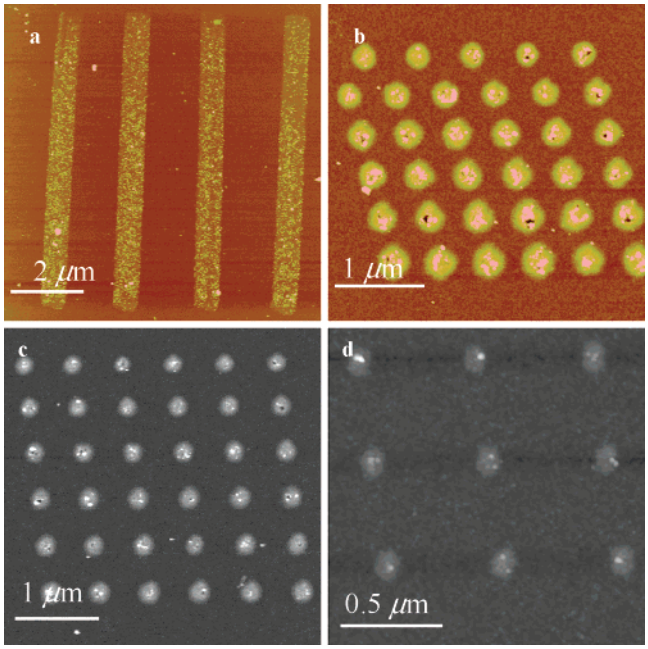

Figure 3. AFM images of different oxide templates on APTMS−Si substrate after immersion in SDS-modified $Fe(OH)_3$ solution for 5 min: (a) some straight lines and (b, c, d) some dot arrays with different domain size.

the concentration of SDS molecules in the system was high enough to form hemi-micelle or bilayerlike structures (although the layers were not compact and uniform) which act as a "resist" preventing direct interaction between $Fe(OH)_3$ nanoparticles and the amino-covered surface layer. After being washed in deionized water, both SDS molecules and $Fe(OH)_3$ nanoparticles were removed. Furthermore, as indicated in Figure 3d, the critical size of oxide dot was much larger than that in SDS free solution, which means that the size of the oxide dot should be large enough (more than 100 nm) to anchor $Fe(OH)_3$ nanoparticles. This value is also larger than the size of very small pinholes in the layer that can act as reactive sites for nanoparticle adsorption.

Immersing the wafers either in $Fe(OH)_3$ solution or SDS-containing $Fe(OH)_3$ solution produced considerable adsorption of $Fe(OH)_3$ onto the oxide nanodomains (Figure 3). This indicates that oxide nanodomains were negatively charged when the sample was immersed in the modified solution, and there is no SDS adsorption because of the repulsive electrostatic force. However, $Fe(OH)_3$ nanoparticles still have a great affinity to the oxide nanodomains due to electrostatic forces and/or hydrogen bond forces (FeO···HOSi).

The ratio (v/v) of SDS to $Fe(OH)_3$ solution is crucial for the selective deposition of nanoparticles onto oxide nanodomains. With excess SDS there would be no particle deposition on either oxide nanodomains or the bulk substrate surface. This was due to the fact that there would be no attractive forces between the particles and the oxide nanodomains. On the other hand, excess $Fe(OH)_3$ would lead to flocculation of the colloid. It was found that freshly prepared SDS containing solution was metastable and would flocculate within several hours. ζ potential of such solutions was close to 0 V. And freshly prepared SDS-containing solution was required for every experimental run.

To validate the SDS-resist mechanism, another SAM, OTS-coated Si substrate was patterned by SPO and used as a substrate to adsorb nanoparticles. The OTS SAM-coated Si substrate was first immersed in $Fe(OH)_3$ solution without SDS, and the result was similar to that of APTMS-coated Si substrate in that many nanoparticles adsorbed on the entire surface of the substrate,

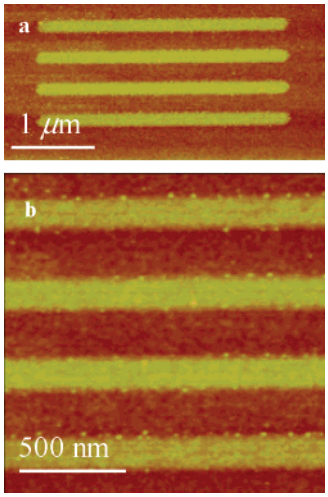

Figure 4. (a) AFM images of probe scanned lines on OTS−Si surface after immersion in SDS-modified $Fe(OH)_3$ solution for 5 min and (b) its magnified image.

which was due to the physisorption of hydroxide ions from the aqueous solution.[28] Immersing patterned OTS-coated Si substrate in SDS-containing $Fe(OH)_3$ solutions would result in selective adsorption of $Fe(OH)_3$ nanoparticles onto SPO-defined nanodomains. For that under these conditions compact and uniform SDS monolayers would be formed on hydrophobic SAMs.[26] As might be expected, almost no particles were seen on the bulk of the OTS-covered substrate (Figure 4) and many nanoparticles were selectively absorbed at the boundaries of SPO defined areas. The boundary effect has been discussed in detail elsewhere,[23] briefly, water bridging the AFM tip and sample would work as an electrochemical nanocell providing oxygen species for oxide growth. The hydrophobic nature of OTS and an inefficient water supply would favor the formation of Si−O−Si bonds on the oxide domain centers. The oxidation of domain boundaries on the other hand would take place in a relatively weak electrical field because of the more open environment, facilitating water supply and promoting the formation of Si−OH bonds. As depicted above, it is the attraction between nanoparticles and Si−OH that assembles $Fe(OH)_3$ onto oxide regions.

C. SWNT Growth. By using various iron-containing nanoparticles (Fe, Fe/Mo, Fe/Ru) and a suitable carbon source, isolated SWNTs have been successfully produced on SiO_2 (normally $t_{ox} > 100$ nm) coated Si substrates.[10−14] However, there have been relatively few reports on the growth of single SWNTs on Si (or native oxide-coated Si) substrates.[29] This is due to inappropriate interaction/reaction between nanoparticles and the underlying substrate.[30,31] Jung et al. investigated the reason for lack of MWNTs growth on Si substrates using several high-resolution techniques (HRTEM, selective area electron beam diffraction, etc.). They demonstrated that, during high-temperature processing, catalytically inactive iron silicide ($FeSi_2$)/iron silicate ($FeSiO_4$) particles formed on the Si substrate.[30] Combining in situ XPS and UPS findings, Prabhakaran et al. proposed that nanoparticle catalysts present on the Si region were poisoned as a result of the formation of a silicon oxide layer encapsulating the particle. This encapsulation phenomenon results in the sinking of catalyst nanoparticles beneath a thin layer of SiO_2, inhibiting their catalytic activity.[31]

On SiO_2 ($t_{ox} = 600$ nm) coated Si substrates, iron oxide nanoparticles produced by decomposition of $Fe(OH)_3$ have been used to catalyze the growth of SWNTs.[32] The diameter distributions of iron-containing nanoparticles and SWNTs were

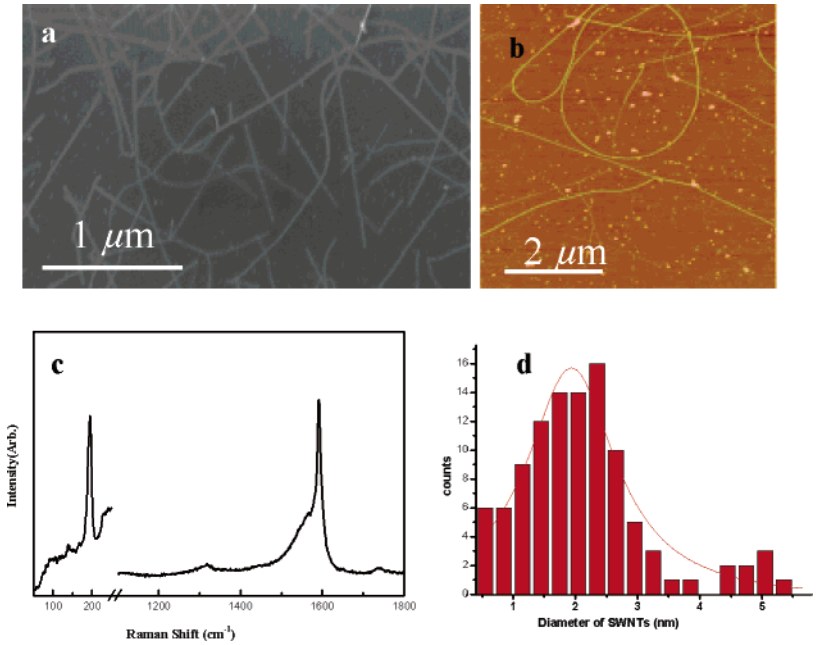

Figure 5. (a) SEM image of carbon nanotubes grown on an SiO_2 surface with $CH_4 = 600$ sccm at 900 °C for 10 min. (b) An AFM image of carbon nanotube grown on Si substrate. (c) A typical resonant Raman spectrum taken from the SWNTs grown on Si substrates. (d) Diameter distribution of SWNTs grown on Si substrate.

demonstrated in that report (the diameter distribution of the catalytic nanoparticles showed a peak centered at 1.8 nm with 93% in the range 1−5 nm). On Si substrates, to our surprise, SWNTs can also grow from the catalytic nanoparticles. Figure 5a shows a SEM image of carbon nanotubes grown on Si substrate by CVD with CH_4 for 10 min at 900 °C. Many tubes can be seen growing on the substrate. From the AFM image (Figure 5b), however, it can be seen that growth efficiency was low (<1%) compared with those grown on a SiO_2 substrate. A resonance Raman spectrum taken from the substrate is shown in Figure 5c: the RBM peak lies at 195 cm^{-1} proving the existence of SWNTs, while the relatively low intensity of the D-band accounted for the high-purity carbon nanotubes with almost no defects. The diameter of carbon nanotubes was determined by AFM. Figure 5d shows the diameter distribution of carbon nanotubes: a center diameter lies at 1.9 nm while diameters ranged from 0.4 to 3.0 nm. This result is consistent with the size distribution of iron oxide nanoparticles and implies that controlling the diameter of catalytic nanoparticles may be an effective way of determining the diameters of SWNTs. Nanotubes with much larger diameter (>5 nm) were also obtained but these seemed to be small SWNT bundles or multiwalled carbon nanotubes.

For future applications of SWNT, it is important to grow SWNTs directly from predetermined nanodomains; the key issue is how to precisely position catalyst nanoparticles. Using SDS as a resist has shown the possibility of precisely locating SPO nanodomains and thus locating $Fe(OH)_3$ catalytic nanoparticles. After annealing for half an hour in air at 600 °C, the SAM and residual SDS were burned away and $Fe(OH)_3$ nanoparticles were converted to iron oxide, with no change in position. They were then used as catalyst for growing SWNTs, although the growth efficiency was not high (Figure 6). Figure 6a,b,c also demonstrates the growth of SWNTs from SPO-defined lines, where many nanotubes protrude from the iron-containing catalytic nanoparticles. Comparing with Figure 3a, clear evidence is provided for the base-growth mode of SWNTs on Si substrates at precisely predetermined locations based on the position of catalytic nanoparticles. Figure 6d shows AFM images of

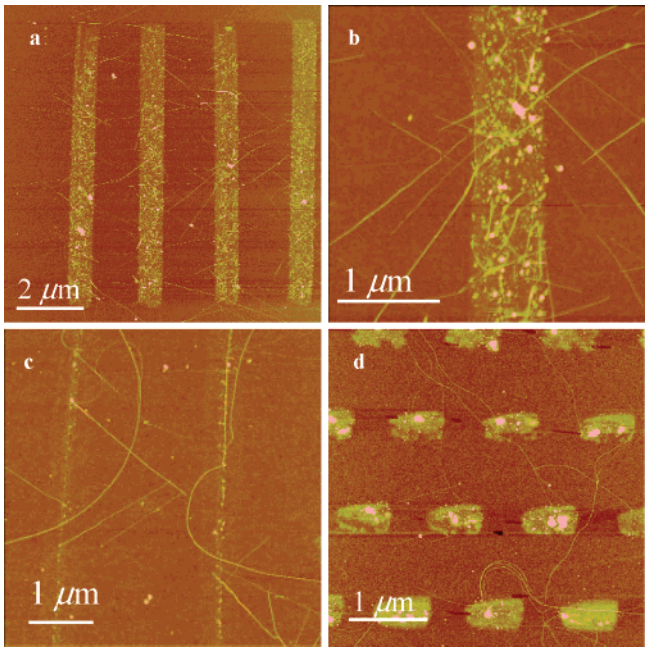

Figure 6. (a) An AFM image of SWNTs grown from probe-scanned lines from iron-containing catalyst and (b) its magnified image. (c) An AFM image of SWNTs grown out from thinner particle lines. (d) An AFM image of SWNTs grown from SPO defined dot arrays.

SWNTs grown from nanoparticles on patterned oxide nanodomains. Although multitime growth periods have proved successful in greatly enhancing the growth efficiency of catalyst nanoparticles on SiO_2 substrates,[32] it was not effective here. This was due to poisoning of the catalyst: on SiO_2 substrate, the catalyst nanoparticle was poisoned mainly by a coating of amorphous carbon which, however, could be burned away at 450 °C in air for half an hour, thus reactivating it as a catalyst for further growth of SWNTs. On Si substrate, however, the catalyst was poisoned due to a coating of SiO_2 or formation of silicide, and could not be easily reactivated. Further work will

be done to enhance the growth efficiency of catalyst nanoparticles on Si substrate.

Conclusions

In summary, resisted with SDS, sub-5 nm $Fe(OH)_3$ nanoparticles have been successfully assembled onto SPO-defined patterns on SAM-coated Si substrate. The number and location of nanoparticles that assembled onto oxide patterns was related to the size of the pattern and the wettability properties of SAM. This surfactant-resisted mechanism may be applied for other nanoobjects assembly that is required for ultimate nanostructuring. And also, after being annealed in air, the iron-containing nanoparticles acted as a catalyst for CVD growth of SWNTs on the basis of base growth mode. This site-specific growth of SWNTs is expected to promote the research and development of high-performance SWNT-based electronic devices.

Acknowledgment. This work was supported by the National Natural Science Foundation of China (NSFC 90206023), the Ministry of Science and Technology of China (2001CB6105), and the FOKYING TUNG Education Foundation (94012). We are grateful to Prof. C Robinson (University of LEEDS, UK) for his kind help and useful discussion.

References and Notes

(1) Ajayan, P. M. *Chem. Rev*. **1999**, *99*, 1787.
(2) Bethune, D. S.; Kiang, C. H.; de Vries, M. S.; Gorman, G.; Savoy, R.; Vazquez, J.; Beyers, R. *Nature* **1993**, *363*, 605.
(3) Thess, A.; Lee, R.; Nikolaev, P.; Dai, H. J.; et al. *Science* **1996**, *273*, 483.
(4) Kong, J.; Cassell, A. M.; Dai, H. *Chem. Phys. Lett.* **1998**, *292*, 567.
(5) Tans, S. J.; Devoret, M. H.; Dai, H. J.; Thess, A.; Smalley, R. E.; Geerligs, L. J.; Dekker, C. *Nature* **1996**, *386*, 474.
(6) Martel, R.; Schmidt. T.; Shea, H. R.; Hertel, T.; Avouris, P. *Appl. Phys. Lett.* **1998**, *73*, 2447.
(7) Postma, H. W. C.; Teepen, T.; Yao, Z.; Grifoni, M.; Dekker: C. *Science* **2001**, *293*, 76.
(8) Dai, H. *Acc. Chem. Res.* **2002,** *35*, 1035.
(9) Liu, J.; Fan, S. S.; Dai, H. J. *Mater. Res. Soc. Bull.* **2004**, *29*, 244.
(10) Cheung, C. L.; Kurtz, A.; Park, H.; Lieber, C. M. *J. Phys. Chem. B* **2002**, *106*, 2429.
(11) An, L.; Owens, J. M.; McNeil, L. E.; Liu, J. *J. Am. Chem. Soc.* **2002**, *124*, 13688.
(12) Choi, H. C.; Kim, W.; Wang, D. W.; Dai, H. *J. Phys. Chem. B* **2002**, *106*, 12361.
(13) Huang, S. M.; Cai, X. Y.; Liu, J. *J. Am. Chem. Soc.* **2003**, *125*, 5636.
(14) Joselevich, E.; Lieber, C. M. *Nano Lett.* **2002**, *2*, 1137.
(15) Zhang, Y. G.; Chang, A.; Cao, J.; Wang, Q.; et al. *Appl. Phys. Lett.* **2001**, *79*, 3155.
(16) Kong, J.; Soh, H.; Cassell, A.; Quate, C. F.; Dai, H. J. *Nature* **1998**, *395*, 878.
(17) Cassell, A. M.; Franklin, N. R.; Tombler, T. W.; Chan, E. M.; Han, J.; Dai, H. J. *J. Am. Chem. Soc.* **1999**, *121*, 7975.
(18) Teberio, R. C.; Craighead, H. G.; Lercel, M.; Lau, T.; Sheen, C. W.; Allara, D. L. *Appl. Phys. Lett.* **1993**, *62*, 476.
(19) Wollman, E. W.; Kang, D.; Frisbie, C. D.; Lorkovic, I. M.; Wrighton, M. S. *J. Am. Chem. Soc.* **1994**, *116*, 4395.
(20) Kramer, S.; Fuierer, R. R.; Gorman, C. B. *Chem. Rev*. **2003**, *103*, 4367.
(21) Liu, S. T.; Maoz, R.; Schmid, D.; Sagiv, J. *Nano Lett.* **2002**, *2*, 1055.
(22) Sugimura, H.; Hozumi, A.; Kameyama, T.; Takai, O. *Surf. Interface Anal.* **2002**, *34*, 550.
(23) Ling, X.; Zhu, X.; Zhang, J.; Zhu, T.; Liu, M. H.; Tong, L. M.; Liu, Z. F. *J. Phys. Chem. B* **2005**, *109*, 2657.
(24) Li, Q. G.; Zheng, J. W.; Liu, Z. F. *Langmuir* **2003**, *19*, 166.
(25) Zhang, H.; He, H. X.; Wang, J.; Mu, T.; Liu, Z. F. *Appl. Phys. A* **1998**, *66*, S269.
(26) Brus, L. *Nature* **1991**, *351*, 301.
(27) Hu, K.; Bard, A. J. *Langmuir* **1997**, *13*, 5418.
(28) Zangi, R.; Engbets, B. *J. Am. Chem. Soc.* **2005**, *127*, 2272.
(29) Kobayashi, Y.; Nakashima, H.; Takagi, D.; Homma, Y. *Thin Solid Films* **2004**, *484*−*485*, 286.
(30) Jung, Y. J.; Wei, B. Q.; Vajtai, R.; Ajayan, P. M.; Homma, Y.; Prabhakaran, K.; Ogino, T. *Nano Lett.* **2003**, *3*, 561.
(31) Prabhakaran, K.; Watanabe, Y.; Homma, Y.; Ogino, T.; et al. *Langmuir* **2003,** *19*, 10629.
(32) He, M. S.; Duan, X. J.; Wang, X.; Zhang, J.; Liu, Z. F.; Robinson, C. *J. Phys. Chem. B* **2004**, *108*, 12665.